2020 IEEE/RSJ International Conference on Intelligent Robots and Systems (IROS)
October 25-29, 2020, Las Vegas, NV, USA (Virtual)

A Variable Impedance Control Strategy for Object Manipulation Considering Non–Rigid Grasp

Michalis Logothetis[1], George C. Karras[2,1], Konstantinos Alevizos[1] and Kostas J. Kyriakopoulos[1]

***Abstract*— This paper presents a novel control strategy for the compensation of the slippage effect during non-rigidly grasped object manipulation. A detailed dynamic model of the interconnected system composed of the robotic manipulator, the object and the internal forces and torques induced by the slippage effect is provided. Next, we design a model-based variable impedance control scheme, in order to achieve simultaneously zero convergence for the trajectory tracking error and the slippage velocity of the object. The desired damping and stiffness matrices are formulated online, by taking into account the measurement of the slippage velocity on the contact. A formal Lyapunov-based analysis guarantees the stability and convergence properties of the resulting control scheme. A set of extensive simulation studies clarifies the proposed method and verifies its efficacy.**

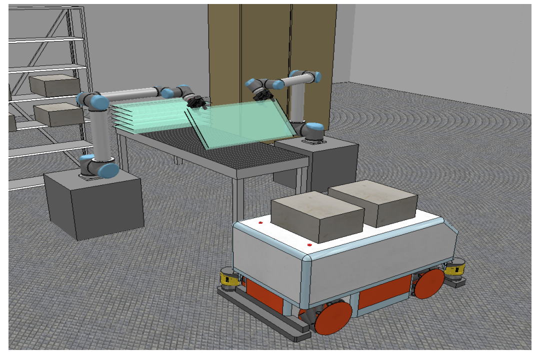

Fig. 1: Cooperative Transportation Tasks of Fragile Objects.

I. Introduction

During the last decades, a significant increase of robots employment in various fields of industry has been noted, including production, logistics and manufacturing [1], [2]. In most cases, robots frequently interact with delicate cargo objects, tools or sophisticated equipment (e.g medical robots). In this vein, safe and precise autonomous object manipulation is an important robotic operation which requires a set of precise detection, recognition and grasping control algorithms.

Numerous studies have been reported regarding the design of object manipulation control strategies for either single or cooperative robotic systems [3]–[8]. Despite the fact that early works are focused on centralized control architectures [3], [4], the need to employ large-scale interconnected robotic systems able to accomplish complex tasks, has concentrated the recent studies on decentralized control approaches [5]–[8].

However, most research efforts consider a *rigid* contact between the robots' end-effector and the grasped object. In practice, this assumption can be unrealistic for certain object classes such as in cases where two manipulators are employed in order to grasp and cooperatively transport a bulky fragile item (e.g a glass frame) across an assembly line as depicted in Fig. 1. In such case, the gripping as well the induced internal forces must be considerably low in order to prevent damage or complete destruction of the object, making the assumption of contact rigidity invalid and the relevant manipulation techniques unsuitable for this kind of application.

Nevertheless, *non–rigid* manipulation is a rather challenging undertaking, mainly due to the absence of contact constraints on the slippy directions of the object, that significantly increase the complexity of the system model. Research efforts that tackle the problem of non-rigid contact during object manipulation are still limited in comparison to the rigid contact ones and can be distinguished in two main categories: a) methods that focus on slippage detection via sensor development and b) methods that compensate the slippage effect via the design of appropriate control strategies.

Different sensor technologies have been employed in order to provide accurate and robust slippage detection, with tactile sensing being one of the leading approaches [9]. Early slip sensors were based on accelerometers or similar technologies, able to detect small, transient forces or motions with increased sensitivity [10]. Moreover, a few attempts to integrate optical and pressure sensors [11] have been reported in the literature. Other approaches for slip detection are based on acoustic sensors [12]. Additionally, some examples of slip sensors based on piezo-resistive materials [13] or image processing techniques [14] can also be found in the literature.

From a control point of view, the assumption of a rigid contact between the robot's end-effector and the object, may lead to undesirable behavior of the combined system such as instability, convergence error and safety issues. Thus, the choice of applied forces on the object is of utmost importance in robot manipulation, so as to avoid or minimize the risk of slippage [15], [16]. Recent works use the sliding motion for object re-grasping [17] or in-hand manipulation [18]. In [19], two algorithms are proposed for object and gripper pivoting. Using force and moment measurement, the initial position of the fingers with respect to the object center of gravity and the knowledge of the friction model parameters, the proposed algorithms counteract the slippage velocity by modulation of the grasp force of a gripper. In [20], a three-level slip prevention strategy for dual-arm manipulation is proposed by applying dynamic adjustment of squeeze force, desired motion trajectory and berthing contact force modification. However, they assume that the surface friction coefficients are a priori known.

A manipulation control scheme which considers the slippage between the robot finger tips and the object, is presented

[1]Control Systems Lab, Department of Mechanical Engineering, National Technical University of Athens, 9 Heroon Polytechniou Street, Zografou 15780, Greece. Email: {logothm,kosalevizos,kkyria}@mail.ntua.gr

[2]Dept. of Computer Science and Telecommunications,University of Thessaly, 3rd Km Old National Road Lamia Athens, 35100, Lamia, Greece. Email: gkarras@uth.gr

The research work was supported by the Hellenic Foundation for Research and Innovation (H.F.R.I.) under the First Call for H.F.R.I. Research Projects to support Faculty members and Researchers and the procurement of high-cost research equipment grant (Project Number: HFRI-FM17-466).

978-1-7281-6211-9/20/$31.00 ©2020 IEEE

in [21], [22]. In these studies, the authors are using a model for frictional contact condition, where the slippage equations of motion are considered as a second-order differential system, with known switching coefficients. However, even with the increasing development of tactile sensors, the accurate knowledge of the friction model or its coefficients, is still a non-realistic assumption, especially considering the heterogeneity of robots and objects involved in industrial related applications.

In this work, we address the problem of object manipulation in non-rigid grasp. More specifically, for a rigid object with known dynamics, which is grasped by n_C slippy contacts, we propose a Variable Impedance Control (VIC) strategy, in order to achieve simultaneously guaranteed convergence to zero for the trajectory tracking error and the slippage velocity assuming that no external forces or torques acting on the interconnected system. The dynamic properties of the system are formulated accordingly, by employing the measurements of the slippage velocity and the forces/torques acting on the object, hence the proposed model-based controller ensures a safe, reliable and slippage-free behavior with guaranteed steady state performance. Additionally, a compensation term is added to the system which significantly contributes on the reduction of the slippage effect. At this point, we should highlight that neither the model of friction nor the coefficients between the robot end-effector and the object are considered known, increasing in this way the applicability of the proposed scheme in real case scenarios. Moreover, the slippage velocity that is needed for the proposed controller, can be acquired by using tactile slip sensors similar to the ones proposed in [14], [23].

The rest of the paper is organized as follows: In Sec. II, the dynamic modeling of the combined system is described, including the robot and object dynamic equations, the contact kinematics and the dynamics of the slippage effect. Sec. III presents the design of the proposed Lyapunov-based control scheme along with a stability proof. Sec. IV demonstrates the applicability and performance of the proposed controller via extensive simulation tests. Finally, Sec. V concludes the paper.

II. Mathematical Modeling

In this section, the dynamic equations of the robotic manipulator, the object and the slippage effect are initially presented. A vector ${}^{c}\boldsymbol{x}_{a,b}$ represents the quantity of the difference between the frame $\{a\}$ and $\{b\}$ as observed by the reference frame $\{c\}$. For example, in Fig. 2 the ${}^{o}\boldsymbol{x}_{o,p}$ is the position vector from frame $\{o\}$ to $\{p\}$ as observed by $\{o\}$. When the left upper superscript is absent, we denote that vector is expressed in the world fixed coordinate frame $\{w\}$ and, additionally, if the low left subscript is absent, we denote that the vector is observed and measured by the right upper superscript (${}^{o}\boldsymbol{x}_p \equiv {}^{o}\boldsymbol{x}_{o,p}$ and $\boldsymbol{x}_p \equiv {}^{w}\boldsymbol{x}_{w,p}$).

A. Robot Dynamics

The dynamic model of a manipulator with n_Q number of joints can be written as [24]:

$$\boldsymbol{B}(\boldsymbol{q})\ddot{\boldsymbol{q}} + \boldsymbol{C}(\boldsymbol{q},\dot{\boldsymbol{q}})\dot{\boldsymbol{q}} + \boldsymbol{g}(\boldsymbol{q}) = \boldsymbol{u} + \boldsymbol{J}^{\top}(\boldsymbol{q})\boldsymbol{h}_{ee} \quad (1)$$

,where $\boldsymbol{q}, \dot{\boldsymbol{q}}, \ddot{\boldsymbol{q}} \in \mathbb{R}^{n_Q}$ are the joint position, velocity and acceleration, respectively. $\boldsymbol{B}(\boldsymbol{q}), \boldsymbol{C}(\boldsymbol{q},\dot{\boldsymbol{q}}) \in \mathbb{R}^{n_Q \times n_Q}$ are the mass-inertia matrix and centrifugal and Coriolis terms matrix, respectively. Moreover, $\boldsymbol{g}(\boldsymbol{q}) \in \mathbb{R}^{n_Q}$ is the vector of gravity terms, $\boldsymbol{h}_{ee} \in \mathbb{R}^6$ the vector of interaction forces and torques between the robot end-effector and the environment and $\boldsymbol{u} \in \mathbb{R}^{n_Q}$ is the torque control input induced by the joint motors. The pose of the end-effector w.r.t. world frame $\{w\}$ is denoted as $\boldsymbol{p}_{ee} \in \mathbb{R}^6$ (if we consider Euler angles as orientation representation) and can be computed using forward kinematics:

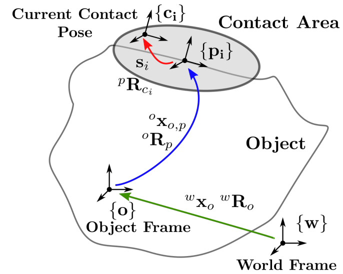

Fig. 2: Contact Area Frames.

$$\boldsymbol{p}_{ee} = \boldsymbol{\mathcal{A}}(\boldsymbol{q}) \quad (2)$$

where $\boldsymbol{\mathcal{A}}(\cdot) : \mathbb{R}^{n_Q} \mapsto \mathbb{R}^6$. The differential kinematics equation is:

$$\dot{\boldsymbol{p}}_{ee} = \boldsymbol{J}_a(\boldsymbol{q})\dot{\boldsymbol{q}} \quad (3)$$

where $\boldsymbol{J}_a(\boldsymbol{q})$ is the analytical jacobian. It holds that:

$$\boldsymbol{J}(\boldsymbol{q}) = \begin{bmatrix} \boldsymbol{\mathcal{I}}_{3\times3} & \mathbf{O}_3 \\ \mathbf{O}_3 & \boldsymbol{T}_\phi(\boldsymbol{\phi}_{ee}) \end{bmatrix} \boldsymbol{J}_a(\boldsymbol{q}) = \underline{\boldsymbol{T}_\phi(\boldsymbol{\phi}_{ee})}\boldsymbol{J}_a(\boldsymbol{q}) \quad (4)$$

where $\boldsymbol{T}_\phi(\boldsymbol{\phi}_{ee}) \in \mathbb{R}^{3\times3}$ is a transformation matrix which definition depends on the euler angle vector $\boldsymbol{\phi}_{ee} \in \mathbb{R}^3$. The relation between the time derivative of the pose of the end–effector $\dot{\boldsymbol{p}}_{ee} = [\dot{\boldsymbol{x}}_{ee}^{\top}, \dot{\boldsymbol{\phi}}_{ee}^{\top}]^{\top} \in \mathbb{R}^6$ and the spatial velocity $\boldsymbol{v}_{ee} = [\dot{\boldsymbol{x}}_{ee}^{\top}, \boldsymbol{\omega}_{ee}{}^{\top}]^{\top} \in \mathbb{R}^6$ is:

$$\boldsymbol{v}_{ee} = \begin{bmatrix} \boldsymbol{\mathcal{I}}_{3\times3} & \mathbf{O}_3 \\ \mathbf{O}_3 & \boldsymbol{T}_\phi(\boldsymbol{\phi}_{ee}) \end{bmatrix} \dot{\boldsymbol{p}}_{ee} = \underline{\boldsymbol{T}_\phi(\boldsymbol{\phi}_{ee})}\dot{\boldsymbol{p}}_{ee} \quad (5)$$

Moreover, the relationship between the angular acceleration and the second time derivative of euler angles is given by:

$$\dot{\boldsymbol{\omega}}_{ee} = \boldsymbol{T}_\phi(\boldsymbol{\phi}_{ee})\ddot{\boldsymbol{\phi}}_{ee} + \dot{\boldsymbol{T}}_\phi(\boldsymbol{\phi}_{ee}, \dot{\boldsymbol{\phi}}_{ee})\dot{\boldsymbol{\phi}}_{ee} \quad (6)$$

Therefore, it holds that:

$$\boldsymbol{v}_{ee} = \boldsymbol{J}(\boldsymbol{q})\dot{\boldsymbol{q}} \quad (7)$$

Deriving the Eq. 7, we get:

$$\dot{\boldsymbol{v}}_{ee} = \boldsymbol{J}(\boldsymbol{q})\ddot{\boldsymbol{q}} + \dot{\boldsymbol{J}}(\boldsymbol{q})\dot{\boldsymbol{q}} \quad (8)$$

Using the Eq. 7 and Eq. 8, we can express the dynamic model equation in Cartesian Space:

$$\boldsymbol{B}_x(\boldsymbol{q})\dot{\boldsymbol{v}}_{ee} + \boldsymbol{C}_x(\boldsymbol{q},\dot{\boldsymbol{q}})\boldsymbol{v}_{ee} + \boldsymbol{g}_x(\boldsymbol{q}) = \boldsymbol{u}_{C,x} + \boldsymbol{h}_{ee} \quad (9)$$

where $\boldsymbol{B}_x(\boldsymbol{q}) = \boldsymbol{J}^{+\top}\boldsymbol{B}\boldsymbol{J}^{+}$, $\boldsymbol{C}_x(\boldsymbol{q},\dot{\boldsymbol{q}}) = \boldsymbol{J}^{+\top}\boldsymbol{C}\boldsymbol{J}^{+} - \boldsymbol{B}_x\dot{\boldsymbol{J}}\boldsymbol{J}^{+}$, $\boldsymbol{g}_x(\boldsymbol{q}) = \boldsymbol{J}^{+\top}\boldsymbol{g}$ and $\boldsymbol{u}_{C,x} = \boldsymbol{J}^{+\top}\boldsymbol{u}$. With the right superscript $({}^{+})$ we denote the Moore-Penrose pseudo-inverse or the inverse of a matrix if it is non-square or square, respectively. Then, the properties of the dynamic model still hold assuming that the $\boldsymbol{J}$ is non singular.

B. Object Dynamics

The dynamics of a rigid object expressed in world frame $\{w\}$ can be obtained by:

$$\boldsymbol{B}_o\dot{\boldsymbol{v}}_o + \boldsymbol{C}_o(\boldsymbol{v}_o)\boldsymbol{v}_o + \boldsymbol{g}_o(\boldsymbol{p}_o) = -\boldsymbol{h}_o \quad (10)$$

where:

$$\boldsymbol{B}_o = \begin{bmatrix} m_o\boldsymbol{\mathcal{I}}_{3\times3} & \mathbf{O}_3 \\ \mathbf{O}_3 & \boldsymbol{\mathcal{J}}_o \end{bmatrix} \in \mathbb{R}^{6\times6}, \boldsymbol{\mathcal{J}}_o \in \mathbb{R}^{3\times3}$$

$$\boldsymbol{C}_o(\boldsymbol{v}_o) = \begin{bmatrix} \mathbf{O}_3 & \mathbf{O}_3 \\ \mathbf{O}_3 & \boldsymbol{S}(\boldsymbol{\omega}_o)\boldsymbol{\mathcal{J}}_o \end{bmatrix} \in \mathbb{R}^{6\times6},\ \boldsymbol{h}_o = \sum_{i=1}^{n_C}\left\{\boldsymbol{G}_i\boldsymbol{h}_{eei}\right\} \in \mathbb{R}^6$$

,where $\boldsymbol{p}_o = [\boldsymbol{x}_o{}^{\top}, \boldsymbol{\phi}_o{}^{\top}]^{\top} \in \mathbb{R}^6$, $\boldsymbol{v}_o = [\dot{\boldsymbol{x}}_o^{\top}, \boldsymbol{\omega}_o{}^{\top}]^{\top} \in \mathbb{R}^6$, $\dot{\boldsymbol{v}}_o = [\ddot{\boldsymbol{x}}_o^{\top}, \dot{\boldsymbol{\omega}}_o^{\top}]^{\top} \in \mathbb{R}^6$ is the 3D pose, spatial velocity and acceleration of the object. $\boldsymbol{h}_o$ is the sum of the generalized forces exerted by the manipulator on the object. The $\boldsymbol{G}_i \in \mathbb{R}^{6\times6}$ is the partial grasp matrix which definition will be analyzed in the following sections.

C. Contact Kinematics Considering Slippage

Consider an object with reference frame $\{o\}$ located on its Center of Mass (COM) and $\{w\}$ the world frame. We define $i = 1 \dots n_C$ contact points located on the object surface after the initial robot grasp and prior to further motion. For each contact point, we define an initial frame $\{p_i\}$ describing the pose of the i^{th} contact point before slippage. Since the object is rigid, the position of each initial contact point w.r.t COM can be considered constant, hence ${}^{o}\boldsymbol{x}_{p_i} \equiv {}^{o}\boldsymbol{x}_{o,p_i} =$ const. During the manipulator motion, the slippage effect is induced, and the contact points are now moving along the object surface with $\{c_i\}$ the frames denoting the relative motion w.r.t to the initial grasping frames $\{p_i\}$. The slippage position ${}^{p_i}\boldsymbol{x}_{p_i,c_i} \equiv {}^{p_i}\boldsymbol{s}_{il} \neq 0$, linear velocity ${}^{p_i}\dot{\boldsymbol{x}}_{p_i,c_i}(t) \equiv {}^{p_i}\boldsymbol{v}_{sil}$ and linear acceleration ${}^{p_i}\ddot{\boldsymbol{x}}_{p_i,c_i}(t) \equiv {}^{p_i}\dot{\boldsymbol{v}}_{sil}$ can be defined as continuous functions of time. Where ${}^{p_i}\boldsymbol{s}_i = [{}^{p_i}\boldsymbol{s}_{il},\ {}^{p_i}\boldsymbol{s}_{ia}] \in \mathbb{R}^6$ is the slippage displacement considering euler angles to represent the orientation. Then, ${}^{p_i}\boldsymbol{v}_{si} = [\boldsymbol{v}_{sil}, \boldsymbol{v}_{sia}] = \underline{\boldsymbol{T}_{\phi}({}^{p_i}\boldsymbol{s}_{ia})}{}^{p_i}\dot{\boldsymbol{s}}_i \in \mathbb{R}^6$. The kinematic equation of the point $\{c_i\}$ w.r.t. $\{w\}$ frame can be calculated as:

$$\boldsymbol{x}_{c_i} = \boldsymbol{x}_o + {}^{w}\boldsymbol{R}_o {}^{o}\boldsymbol{x}_{,p_i} + {}^{w}\boldsymbol{R}_o {}^{o}\boldsymbol{R}_{p_i} {}^{p_i}\boldsymbol{s}_{il} \tag{11}$$

,where ${}^{w}\boldsymbol{x}_{w,c_i} \equiv \boldsymbol{x}_{c_i}$, ${}^{w}\boldsymbol{x}_{w,o} \equiv \boldsymbol{x}_o$ and taking into account the Eq. 11. Considering the assumption of a rigid object (${}^{o}\boldsymbol{R}_{p_i} =$ const. $\in \mathbb{R}^{3\times3}$ and ${}^{o}\boldsymbol{x}_{p_i} =$ const. $\in \mathbb{R}^3$) the time derivative of the Eq. 11 is calculated by:

$$\dot{\boldsymbol{x}}_{c_i} = \begin{bmatrix}\boldsymbol{\mathcal{I}}_{3\times3} & \boldsymbol{S}^{\top}(\boldsymbol{x}_{o,p_i} + {}^{w}\boldsymbol{R}_{p_i} {}^{p_i}\boldsymbol{s}_{il})\end{bmatrix} \begin{bmatrix}\dot{\boldsymbol{x}}_o \\ \boldsymbol{\omega}_o\end{bmatrix} + {}^{w}\boldsymbol{R}_{p_i} {}^{p_i}\boldsymbol{v}_{sil} \tag{12}$$

The angular velocity of the contact $\{c_i\}$ with respect to world frame is:

$$\boldsymbol{\omega}_{c_i} = \boldsymbol{\omega}_o + {}^{w}\boldsymbol{R}_{p_i} {}^{p_i}\boldsymbol{v}_{sia} \tag{13}$$

Combining the above equations, the spatial velocity of $\{c_i\}$ is obtained by:

$$\begin{aligned}\boldsymbol{v}_{c_i} &= \begin{bmatrix}\boldsymbol{\mathcal{I}}_{3\times3} & \boldsymbol{S}^{\top}(\boldsymbol{x}_{o,p_i} + {}^{w}\boldsymbol{R}_{p_i} {}^{p_i}\boldsymbol{s}_{il}) \\ \mathbf{O}_{3\times3} & \boldsymbol{\mathcal{I}}_{3\times3}\end{bmatrix} \begin{bmatrix}\dot{\boldsymbol{x}}_o \\ \boldsymbol{\omega}_o\end{bmatrix} + \begin{bmatrix}{}^{w}\boldsymbol{R}_{p_i} & \mathbf{O}_{3\times3} \\ \mathbf{O}_{3\times3} & {}^{w}\boldsymbol{R}_{p_i}\end{bmatrix} \begin{bmatrix}{}^{p_i}\boldsymbol{v}_{sil} \\ {}^{p_i}\boldsymbol{v}_{sia}\end{bmatrix} \\ &= \boldsymbol{G}_i{}^{\top}\boldsymbol{v}_o + \underline{{}^{w}\boldsymbol{R}_{p_i}} {}^{p_i}\boldsymbol{v}_{si}\end{aligned} \tag{14}$$

where, $\boldsymbol{G}_i \in \mathbb{R}^{6\times6}$ is the partial grasp matrix, $\underline{{}^{w}\boldsymbol{R}_{p_i}} = \operatorname{diag}\left({}^{w}\boldsymbol{R}_{p_i}, {}^{w}\boldsymbol{R}_{p_i}\right) \in \mathbb{R}^{6\times6}$ is a diagonal matrix, and $\boldsymbol{v}_{c_i}, \boldsymbol{v}_o \in \mathbb{R}^6$ the spatial velocity of the object and contact point $\{c_i\}$, respectively. In similar way, we get the linear and angular acceleration of the $\{c_i\}$ by:

$$\begin{aligned}\ddot{\boldsymbol{x}}_{c_i} =& \ddot{\boldsymbol{x}}_o + \boldsymbol{S}^{\top}(\boldsymbol{x}_{o,p_i} + {}^{w}\boldsymbol{R}_{p_i} {}^{p_i}\boldsymbol{s}_{il})\dot{\boldsymbol{\omega}}_o + 2\boldsymbol{S}(\boldsymbol{\omega}_o){}^{w}\boldsymbol{R}_{p_i} {}^{p_i}\boldsymbol{v}_{sil} + \\ & \boldsymbol{\omega}_o \times \left(\boldsymbol{\omega}_o \times (\boldsymbol{x}_{o,p_i} + {}^{w}\boldsymbol{R}_{p_i} {}^{p_i}\boldsymbol{s}_{il})\right) + {}^{w}\boldsymbol{R}_{p_i} {}^{p_i}\dot{\boldsymbol{v}}_{sil}\end{aligned} \tag{15}$$

$$\dot{\boldsymbol{\omega}}_{c_i} = \dot{\boldsymbol{\omega}}_o + \boldsymbol{S}(\boldsymbol{\omega}_o){}^{w}\boldsymbol{R}_{p_i} {}^{p_i}\boldsymbol{v}_{sia} + {}^{w}\boldsymbol{R}_{p_i} {}^{p_i}\dot{\boldsymbol{v}}_{sia} \tag{16}$$

Therefore, the spatial acceleration in matrix form is:

$$\begin{aligned}\dot{\boldsymbol{v}}_{c_i} =& \boldsymbol{G}_i{}^{\top}\dot{\boldsymbol{v}}_o + \begin{bmatrix}2\boldsymbol{S}(\boldsymbol{\omega}_o){}^{w}\boldsymbol{R}_{p_i} & \mathbf{O}_{3\times3} \\ \mathbf{O}_{3\times3} & \boldsymbol{S}(\boldsymbol{\omega}_o){}^{w}\boldsymbol{R}_{p_i}\end{bmatrix} {}^{p_i}\boldsymbol{v}_{si} + \underline{{}^{w}\boldsymbol{R}_{p_i}} {}^{p_i}\dot{\boldsymbol{v}}_{si} + \\ & \begin{bmatrix}\boldsymbol{\omega}_o \times \left(\boldsymbol{\omega}_o \times (\boldsymbol{x}_{o,p_i} + {}^{w}\boldsymbol{R}_{p_i} {}^{p_i}\boldsymbol{s}_{il})\right) \\ \mathbf{O}_{3\times1}\end{bmatrix} \\ =& \boldsymbol{G}_i{}^{\top}\dot{\boldsymbol{v}}_o + \boldsymbol{\Phi}_1(\boldsymbol{\omega}_o, {}^{w}\boldsymbol{R}_o){}^{p_i}\boldsymbol{v}_{si} + \underline{{}^{w}\boldsymbol{R}_{p_i}} {}^{p_i}\dot{\boldsymbol{v}}_{si} + \boldsymbol{\Phi}_2(\boldsymbol{\omega}_o, {}^{w}\boldsymbol{R}_o, {}^{p_i}\boldsymbol{s}_{il})\end{aligned} \tag{17}$$

Using the definition of the partial grasp matrix for a non-rigid contact in Eq. 14, it can be easily obtained that:

$$\begin{aligned}\boldsymbol{G}_i &= \begin{bmatrix}\boldsymbol{\mathcal{I}}_{3\times3} & \mathbf{O}_{3\times3} \\ \boldsymbol{S}(\boldsymbol{x}_{o,p_i} + {}^{w}\boldsymbol{R}_{p_i} {}^{p_i}\boldsymbol{s}_{il}) & \boldsymbol{\mathcal{I}}_{3\times3}\end{bmatrix} \\ &= \begin{bmatrix}\boldsymbol{\mathcal{I}}_{3\times3} & \mathbf{O}_{3\times3} \\ \boldsymbol{S}(\boldsymbol{x}_{o,p_i}) & \boldsymbol{\mathcal{I}}_{3\times3}\end{bmatrix} + \begin{bmatrix}\mathbf{O}_{3\times3} & \mathbf{O}_{3\times3} \\ \boldsymbol{S}({}^{w}\boldsymbol{R}_{p_i} {}^{p_i}\boldsymbol{s}_{il}) & \mathbf{O}_{3\times3}\end{bmatrix} \\ &= \boldsymbol{G}_{C,i} + \boldsymbol{G}_{s,i}\end{aligned} \tag{18}$$

,where $\boldsymbol{G}_{C,i} \in \mathbb{R}^{6\times6}$ and $\boldsymbol{G}_{s,i} \in \mathbb{R}^{6\times6}$ is the constant and variant part of the partial grasp matrix which depends on the slippage displacement ${}^{p_i}\boldsymbol{s}_{il}(t) \in \mathbb{R}^3$, respectively.

D. Slippage Dynamics

Using the Eq. 17, we get:

$$\dot{\boldsymbol{v}}_{si} = \dot{\boldsymbol{v}}_{c_i} - \boldsymbol{G}_i{}^{\top}\dot{\boldsymbol{v}}_o - \boldsymbol{\Phi}_1'\boldsymbol{v}_{si} - \boldsymbol{\Phi}_2 \tag{19}$$

where $\dot{\boldsymbol{v}}_{si} \in \mathbb{R}^6$ is the slippage acceleration wrt $\{w\}$ frame. By substituting the Eq. 9 and Eq. 10 in Eq. 19 and assuming that the end–effector $\{ee\}$ has the same velocity with the moving contact $\{c_i\}$ ($\boldsymbol{v}_{ee} = \boldsymbol{v}_{c_i} \Rightarrow \dot{\boldsymbol{v}}_{ee} = \dot{\boldsymbol{v}}_{c_i}$), we get:

$$\begin{aligned}\dot{\boldsymbol{v}}_{si} =& -\left(\mathcal{P} - \boldsymbol{\Phi}_1'\right)\boldsymbol{v}_{si} - \boldsymbol{C}_{s_i}\boldsymbol{v}_{ee} \\ & + \boldsymbol{g}_{s_i} + \boldsymbol{L}_{s_i}\boldsymbol{h}_{ee} - \boldsymbol{\Phi}_2 + \boldsymbol{B}_x{}^{-1}\boldsymbol{u}_{C,x}\end{aligned} \tag{20}$$

where $\boldsymbol{\Phi}_1' = \begin{bmatrix}2\boldsymbol{S}(\boldsymbol{\omega}_o) & \mathbf{O}_{3\times3} \\ \mathbf{O}_{3\times3} & \boldsymbol{S}(\boldsymbol{\omega}_o)\end{bmatrix} \in \mathbb{R}^{6\times6}$, $\mathcal{P} = \boldsymbol{G}_i{}^{\top}\boldsymbol{B}_o{}^{-1}\boldsymbol{C}_o\boldsymbol{G}_i{}^{-\top} \in \mathbb{R}^{6\times6}$, $\boldsymbol{C}_{s_i} = \left(\boldsymbol{B}_x{}^{-1}\boldsymbol{C}_x - \boldsymbol{G}_i{}^{\top}\boldsymbol{B}_o{}^{-1}\boldsymbol{C}_o\boldsymbol{G}_i{}^{-\top}\right) \in \mathbb{R}^{6\times6}$, $\boldsymbol{g}_{s_i} = \left(\boldsymbol{G}_i{}^{\top}\boldsymbol{B}_o{}^{-1}\boldsymbol{g}_o - \boldsymbol{B}_x{}^{-1}\boldsymbol{g}_x\right) \in \mathbb{R}^6$ and $\boldsymbol{L}_{s_i} = \left(\boldsymbol{G}_i{}^{\top}\boldsymbol{B}_o{}^{-1}\boldsymbol{G}_i + \boldsymbol{B}_x{}^{-1}\right) \in \mathbb{R}^{6\times6}$. We assume that $\boldsymbol{G}_i \in \mathbb{R}^{6\times6}$ and $\boldsymbol{B}_x \in \mathbb{R}^{6\times6}$ are not singular.

III. Control Design

The main objective is to design a control scheme $\boldsymbol{u}_{C,x} \in \mathbb{R}^6$ that drives the system to the desired trajectory and simultaneously minimize the slippage effect on the contact, $\boldsymbol{e}, \dot{\boldsymbol{e}}, \boldsymbol{v}_{si} \to 0$ through time $t \to +\infty$. To achieve this we assume that the external forces acting on the system are zero.

Using feedback linearization technique for the system described in Eq. 9, we choose the control input as follows:

$$\boldsymbol{u}_{C,x} = \boldsymbol{C}_x(\boldsymbol{q}, \dot{\boldsymbol{q}})\boldsymbol{v}_{ee} + \boldsymbol{g}_x(\boldsymbol{q}) - \boldsymbol{h}_{ee} + \boldsymbol{B}_x\boldsymbol{\alpha}_C \tag{21}$$

where $\boldsymbol{\alpha}_C = [\boldsymbol{\alpha}_{Cp}^{\top},\ \boldsymbol{\alpha}_{Co}^{\top}]^{\top} \in \mathbb{R}^6$ constitutes a new control input to be properly designed. We assume that we have the measurement of the interaction forces and torques $\boldsymbol{h}_{ee} \in \mathbb{R}^6$ which are equal to the object dynamics when $\boldsymbol{v}_s \equiv 0$ or the friction forces in direction where slippage occurs. The linearized system is:

$$\dot{\boldsymbol{v}}_{ee} = \boldsymbol{\alpha}_C \Leftrightarrow [\ddot{\boldsymbol{x}}_{ee}^{\top},\ \dot{\boldsymbol{\omega}}_{ee}^{\top}]^{\top} = [\boldsymbol{\alpha}_{Cp}^{\top},\ \boldsymbol{\alpha}_{Co}^{\top}]^{\top} \tag{22}$$

Proposition 1. *Assume the linearized system in Eq. 22, the diagonal 6×6 positive definite matrices $\boldsymbol{M}_D = \operatorname{diag}\{\boldsymbol{M}_{Dp}, \boldsymbol{M}_{Do}\}$, $\boldsymbol{D}_D = \operatorname{diag}\{\boldsymbol{D}_{Dp}, \boldsymbol{D}_{Do}\}$, $\boldsymbol{K}_D = \operatorname{diag}\{\boldsymbol{K}_{Dp}, \boldsymbol{K}_{Do}\}$ and a desired trajectory $\boldsymbol{p}_{ee}^d(t), \dot{\boldsymbol{p}}_{ee}^d(t), \ddot{\boldsymbol{p}}_{ee}^d(t) \in \mathbb{R}^6$. If the function $\Lambda(\boldsymbol{v}_{si}) = [\Lambda_l^{\top}(\boldsymbol{v}_{sil}),\ \Lambda_a^{\top}(\boldsymbol{v}_{sia})]^{\top} : \mathbb{R}^6 \to \mathbb{R}^6$ has the following properties:*

- *$\Lambda_j(\boldsymbol{v}_{sij}) = \boldsymbol{O}_3$, if $\boldsymbol{v}_{sij} = \boldsymbol{O}_3\ \forall j = l, a$.*
- *continuous bounded function in $\mathbb{R}^6$.*

The linear and angular controllers :

$$\begin{aligned}\boldsymbol{\alpha}_{Cp} =& \ddot{\boldsymbol{x}}_{ee}^d + \boldsymbol{M}_{Dp}^{-1}(-\boldsymbol{K}_{Dp}\boldsymbol{e}_p - \boldsymbol{D}_{Dp}\dot{\boldsymbol{e}}_p + \Lambda_l(\boldsymbol{v}_{sil})) \\ \boldsymbol{\alpha}_{Co} =& \dot{\boldsymbol{\omega}}_{ee}^d - \dot{\boldsymbol{T}}_e(\boldsymbol{e}_o)\dot{\boldsymbol{e}}_o + \boldsymbol{T}_e(\boldsymbol{e}_o)\boldsymbol{M}_{Do}^{-1}[-\boldsymbol{K}_{Do}\boldsymbol{e}_o \\ & - \boldsymbol{D}_{Do}\dot{\boldsymbol{e}}_o + \Lambda_a(\boldsymbol{v}_{sia})]\end{aligned} \tag{23}$$

, where $\boldsymbol{T}_e(\boldsymbol{e}_o) = \boldsymbol{R}_{ee}\boldsymbol{T}_{\phi}(\boldsymbol{e}_o)$, $\boldsymbol{e}_p = \boldsymbol{x}_{ee} - \boldsymbol{x}_{ee}^d \in \mathbb{R}^3$, $\boldsymbol{e}_o = 1/2(\boldsymbol{n}_{ee} \times \boldsymbol{n}_{ee}^d + \boldsymbol{o}_{ee} \times \boldsymbol{o}_{ee}^d + \boldsymbol{a}_{ee} \times \boldsymbol{a}_{ee}^d) \in \mathbb{R}^3$, with $\boldsymbol{R}_{ee} = [\boldsymbol{n}_{ee}, \boldsymbol{o}_{ee}, \boldsymbol{a}_{ee}] \in \mathbb{R}^{3\times3}$ and $\boldsymbol{R}_{ee}^d = [\boldsymbol{n}_{ee}^d, \boldsymbol{o}_{ee}^d, \boldsymbol{a}_{ee}^d] \in \mathbb{R}^{3\times3}$ the rotation matrix of the current and desired end-effector orientation, respectively, guarantee that the closed loop system is Input-to-State Stable (ISS).

Proof. Let us consider as a candidate ISS Lyapunov function a scalar positive definite function $\boldsymbol{V}_e(\boldsymbol{e}, \dot{\boldsymbol{e}}) : \mathbb{R}^6 \times \mathbb{R}^6 \mapsto \mathbb{R}$, where $\boldsymbol{V}_e(0, 0) = 0$ and $\boldsymbol{V}_e(\boldsymbol{e}, \dot{\boldsymbol{e}}) > 0$, $\forall\, \boldsymbol{e}(t), \dot{\boldsymbol{e}}(t) \neq 0$. The sum of the kinetic and potential energy satisfies the above properties:

$$\boldsymbol{V}_e = \frac{1}{2}\dot{\boldsymbol{e}}^\top \boldsymbol{M}_D \dot{\boldsymbol{e}} + \frac{1}{2}\boldsymbol{e}^\top \boldsymbol{K}_D \boldsymbol{e} \tag{24}$$

The closed loop system of Eq. 22 using the proposed controller and Eq. 6 is:

$$\boldsymbol{M}_D \ddot{\boldsymbol{e}} = -\boldsymbol{D}_D \dot{\boldsymbol{e}} - \boldsymbol{K}_D \boldsymbol{e} + \Lambda(\boldsymbol{v}_{si}) \tag{25}$$

as shown in [25] where the $\boldsymbol{T}_e(\boldsymbol{e}_o)$ is non singular assuming that no large orientation errors occurs ($\boldsymbol{e}_o = \pm\pi/2$). Substituting Eq. 25 in the time derivative of Eq. 24, we get:

$$\dot{\boldsymbol{V}}_e = -\dot{\boldsymbol{e}}^\top \boldsymbol{D}_D \dot{\boldsymbol{e}} + \dot{\boldsymbol{e}}^\top \Lambda(\boldsymbol{v}_{si}) \tag{26}$$

considering $\Lambda(\boldsymbol{v}_{si})$ as a bounded external input. As Lyapunov gain we choose $\chi_{12}(r) := \lambda_1 r \in \mathcal{K}$ (belongs to class Kappa functions family) with $\lambda_1 \in (0,1)$. Then $\|\dot{\boldsymbol{e}}\| \geq \chi_{12}(\|\Lambda(\boldsymbol{v}_{si})\|)$ implies that :

$$\dot{\boldsymbol{V}}_e \leq -\dot{\boldsymbol{e}}^\top \boldsymbol{D}_D \dot{\boldsymbol{e}} + \frac{1}{\lambda_1}\|\dot{\boldsymbol{e}}\|^2 , \; \lambda_1 \in (0,1) \tag{27}$$

This shows that if we properly choose $\boldsymbol{D}_D \in \mathbb{R}^{6\times 6}$ the Eq. 24 is an ISS Lyapunov function which immediately implies that the closed loop system 25 is ISS with Lyapunov gain $\chi_{12}(r) := \lambda_1 r \in \mathcal{K}$ for $\lambda_1 \in (0,1)$. ■

Then, we have to properly design the function $\Lambda(\boldsymbol{v}_{si})$ to simultaneously compensate the undesired slippage effect.

Proposition 2. *Assume the system in Eq. 20, the positive definite diagonal* 6×6 *matrices* $\boldsymbol{M}_D = \mathrm{diag}\{M_{Dpx}, \cdots, M_{Doz}\}$, $\boldsymbol{D}_D = \mathrm{diag}\{D_{Dpx}, \cdots, D_{Doz}\}$, $\boldsymbol{K}_D = \mathrm{diag}\{K_{Dpx}, \cdots, K_{Doz}\}$ *and a desired trajectory* $\boldsymbol{p}^d_{ee}(t), \dot{\boldsymbol{p}}^d_{ee}(t) \in \mathbb{R}^6$*. If* $\underline{\boldsymbol{T}_e}$ *is non-singular and the gains* $\gamma_{dp}, \gamma_{do}, \gamma_{kp}, \gamma_{ko}, k_s, \alpha > 0$ *are properly designed, the controller in Eq. 21 with:*

$$\begin{aligned}\boldsymbol{\alpha}_C =& \underline{\boldsymbol{T}_e}\boldsymbol{M}_D^{-1}[-\boldsymbol{K}_i(\boldsymbol{v}_{si})\boldsymbol{e} - \boldsymbol{D}_i(\boldsymbol{v}_{si}))\dot{\boldsymbol{e}} \\ &+ \Lambda(\boldsymbol{v}_{si})] + \Theta(\boldsymbol{e}_o, \dot{\boldsymbol{e}}_o)\end{aligned} \tag{28}$$

where:

$$\begin{aligned}\Lambda(\boldsymbol{v}_{si}) =& \boldsymbol{M}_D \underline{\boldsymbol{T}_e}^{-1} \tanh(\alpha\,|\boldsymbol{v}_{si}|)\big[\boldsymbol{\Phi}_2 - k_s \boldsymbol{v}_{si} - \mathcal{P}(\boldsymbol{v}_{ee} - \boldsymbol{v}_{si}) \\ &- \boldsymbol{G}_i{}^\top \boldsymbol{B}_o{}^{-1}(\boldsymbol{g}_o + \boldsymbol{G}_i \boldsymbol{h}_{ee}) - \Theta(\boldsymbol{e}_o, \dot{\boldsymbol{e}}_o)\big]\end{aligned} \tag{29}$$

and

$$K_{pj} = K_{Dpj}\mathrm{e}^{-\gamma_{kp}|u_{slij}|}, \; K_{oj} = K_{Doj}\mathrm{e}^{-\gamma_{ko}|u_{saij}|}, \forall j \in x,y,z$$
$$D_{pj} = D_{Dpj}\mathrm{e}^{-\gamma_{dp}|u_{slij}|}, \; D_{oj} = D_{Doj}\mathrm{e}^{-\gamma_{do}|u_{saij}|}, \forall j \in x,y,z$$

the diagonal elements of the positive definite variable matrices $\boldsymbol{K}_i(\boldsymbol{v}_{si}), \boldsymbol{D}_i(\boldsymbol{v}_{si}) \in \mathbb{R}^{6\times 6}$*, makes the closed loop dynamics of the slippage velocity* $\boldsymbol{v}_{si} = [\boldsymbol{v}_{sil}{}^\top, \, \boldsymbol{v}_{sia}{}^\top]^\top = [u_{lix}, u_{liy}, \cdots, u_{aiy}, u_{aiz}]^\top \in \mathbb{R}^6$ *Input-to-State Stable (ISS).*

Proof. We choose as candidate ISS Lyapunov function $\boldsymbol{V}_s(\boldsymbol{v}_{si})$ for $\boldsymbol{v}_{si}(t)$ the following:

$$\boldsymbol{V}_s = \frac{1}{2}\boldsymbol{v}_{si}{}^\top \boldsymbol{v}_{si} \tag{30}$$

$\boldsymbol{V}_s : \mathbb{R}^6 \to \mathbb{R}_{\geq 0}$ is a continuous differentiable, positive definite function where $\boldsymbol{V}_s(\boldsymbol{v}_{si}) = 0$ if $\boldsymbol{v}_{si} = 0$. The closed loop dynamics of the system in Eq. 20 using the proposed controller are:

$$\begin{aligned}\dot{\boldsymbol{v}}_{si} =& -\big(\mathcal{P} - \boldsymbol{\Phi}_1'\big)\boldsymbol{v}_{si} + \mathcal{P}\boldsymbol{v}_{ee} + \boldsymbol{G}_i{}^\top \boldsymbol{B}_o{}^{-1}\boldsymbol{g}_o \\ &+ \boldsymbol{G}_i{}^\top \boldsymbol{B}_o{}^{-1}\boldsymbol{G}_i \boldsymbol{h}_{ee} - \boldsymbol{\Phi}_2 + \underline{\boldsymbol{T}_e}\boldsymbol{M}_D^{-1}[-\boldsymbol{K}_i(\boldsymbol{v}_{si})\boldsymbol{e} \\ &- \boldsymbol{D}_i(\boldsymbol{v}_{si}))\dot{\boldsymbol{e}} + \Lambda(\boldsymbol{v}_{si})] + \Theta(\boldsymbol{e}_o, \dot{\boldsymbol{e}}_o)\end{aligned} \tag{31}$$

,where $\Theta(\boldsymbol{e}_o, \dot{\boldsymbol{e}}_o) = \begin{bmatrix}\mathbf{O}_3 \\ \dot{\boldsymbol{T}}_e(\boldsymbol{e}_o, \boldsymbol{e}_o)\dot{\boldsymbol{e}}_o\end{bmatrix}$. Substituting the Eq. 31 to the first time derivative of Eq. 30 we get:

$$\begin{aligned}\dot{\boldsymbol{V}}_s =& -\boldsymbol{v}_{si}{}^\top\big(\mathcal{P} - \boldsymbol{\Phi}_1'\big)\boldsymbol{v}_{si} + \boldsymbol{v}_{si}{}^\top \mathcal{P}\boldsymbol{v}_{ee} \\ &+ \boldsymbol{v}_{si}{}^\top \boldsymbol{G}_i{}^\top \boldsymbol{B}_o{}^{-1}\boldsymbol{G}_i \boldsymbol{h}_{ee} + \boldsymbol{v}_{si}{}^\top \boldsymbol{G}_i{}^\top \boldsymbol{B}_o{}^{-1}\boldsymbol{g}_o \\ &- \boldsymbol{v}_{si}{}^\top \boldsymbol{\Phi}_2 + \boldsymbol{v}_{si}{}^\top \underline{\boldsymbol{T}_e}\boldsymbol{M}_D^{-1}[-\boldsymbol{K}_i(\boldsymbol{v}_{si})\boldsymbol{e} \\ &- \boldsymbol{D}_i(\boldsymbol{v}_{si}))\dot{\boldsymbol{e}} + \Lambda(\boldsymbol{v}_{si})] + \boldsymbol{v}_{si}{}^\top \Theta(\boldsymbol{e}_o, \dot{\boldsymbol{e}}_o)\end{aligned} \tag{32}$$

Using Lemma 1, we obtain that:

$$\begin{aligned}\dot{\boldsymbol{V}}_s =& \boldsymbol{v}_{si}{}^\top\big[\mathcal{P}\boldsymbol{v}_{ee} - \mathcal{P}\boldsymbol{v}_{si} + \boldsymbol{G}_i{}^\top \boldsymbol{B}_o{}^{-1}\boldsymbol{g}_o + \boldsymbol{G}_i{}^\top \boldsymbol{B}_o{}^{-1}\boldsymbol{G}_i\boldsymbol{h}_{ee} - \boldsymbol{\Phi}_2 \\ &+ \underline{\boldsymbol{T}_e}\boldsymbol{M}_D^{-1}\big(-\boldsymbol{K}_i\boldsymbol{e} - \boldsymbol{D}_i\dot{\boldsymbol{e}} + \Lambda(\boldsymbol{v}_{si})\big) + \Theta(\boldsymbol{e}_o, \dot{\boldsymbol{e}}_o)\big]\end{aligned} \tag{33}$$

Consequently, it can be easily obtained that when $\boldsymbol{v}_{si} = 0$ then $\dot{\boldsymbol{V}}_s = 0$. Now, we consider the case where $|\boldsymbol{v}_{si}| \neq 0$. Substituting, the proposed definition of $\Lambda(\boldsymbol{v}_{si})$ in Eq. 29, we conclude that:

$$\dot{\boldsymbol{V}}_s = -k_s \boldsymbol{v}_{si}{}^\top \boldsymbol{v}_{si} + \boldsymbol{v}_{si}{}^\top\big[\underline{\boldsymbol{T}_e}\boldsymbol{M}_D^{-1}\big(-\boldsymbol{K}_i\boldsymbol{e} - \boldsymbol{D}_i\dot{\boldsymbol{e}}\big)\big] \tag{34}$$

considering that $|\boldsymbol{v}_{si}| > 0$ and $\alpha >> 0$ so as to $\tanh(\alpha\,|\boldsymbol{v}_{si}|) = 1$.

If we assume that the frictional forces are sufficient in order to stabilize the object against the gravity in steady state, then the closed loop system Eq. 25 is ISS. In this context, the term $\boldsymbol{Z}(\boldsymbol{e}, \dot{\boldsymbol{e}}) = \underline{\boldsymbol{T}_e}\boldsymbol{M}_D^{-1}\big(-\boldsymbol{K}_i(\boldsymbol{v}_{si})\boldsymbol{e} - \boldsymbol{D}_i(\boldsymbol{v}_{si})\dot{\boldsymbol{e}}\big)$ is bounded because $\boldsymbol{e}, \dot{\boldsymbol{e}}, \underline{\boldsymbol{T}_e}$, $K_{ij}(v) : \mathbb{R} \to [K_{D_{ij}}, 0)$ and $D_{ij}(v) : \mathbb{R} \to [D_{D_{ij}}, 0)\; \forall\, i \in p, o$ and $j \in x, y, z$ are bounded terms.

Therefore, we can choose $\chi_{21}(r) := \lambda_2 r \in \mathcal{K}$ for $\lambda_2 \in (0,1)$ as Lyapunov gain. Then $\|\boldsymbol{v}_{si}\| \geq \chi_{21}(\|\boldsymbol{Z}(\boldsymbol{e}, \dot{\boldsymbol{e}})\|)$ implies that $\|\boldsymbol{Z}(\boldsymbol{e}, \dot{\boldsymbol{e}})\| \leq 1/\lambda_2 \|\boldsymbol{v}_{si}\|$ which leads to:

$$\dot{\boldsymbol{V}}_s \leq -k_s\|\boldsymbol{v}_{si}\|^2 + 1/\lambda_2\|\boldsymbol{v}_{si}\|^2 \tag{35}$$

With $k_s > 1/\lambda_2$ for $\lambda_2 \in (0,1)$ the system 31 is ISS with Lyapunov gain $\chi_{21}(r) := \lambda_2 r$. ■

Proposition 3. *The feedback interconnected system (Fig. 3) of the two subsystems Eq. 25 and Eq. 31 is GAS if no external disturbances acting on it.*

Proof. In Proposition 1 and Proposition 2, we have shown that the subsystems are ISS with Lyapunov gain functions $\chi_{12}(r)$ and $\chi_{21}(r)$, respectively. To prove ISS of the interconnection we exploit the small-gain condition $\chi_{12} \circ \chi_{21}(r) < r$ for all $r > 0$. In our case this reduces to :

$$\chi_{12} \circ \chi_{21}(r) = \lambda_1\lambda_2\, r < r, \qquad \forall r > 0$$

since the $\lambda_1, \lambda_2 \in (0,1)$ which implies that the interconnected system is ISS. Then the interconnected system is GAS given that no external disturbances acting on it according to the definition. ■

IV. Simulation Results

The theoretical findings of the proposed work are verified in a 3D dynamic simulation environment provided by Gazebo [26]. However, the interaction dynamics between the object and robot's end-effector are calculated by a simulator that has been developed using Python's SciPy integration library in order to simulate different friction models. More precisely, the interaction forces generated by the algebraic constraints imposed to the object and robot dynamics are computed analytically using the methodology presented in [27]. Then the computed forces are fed to the Gazebo's physics engine. We consider a scenario involving 2D motion in a workspace, where the end-effector of a robotic manipulator has grasped an object with known dynamics, as depicted in Fig. 4. Given a desired trajectory for the interconnected system, the robot tries to move accordingly in order to reach the goal and simultaneously minimize the slip effect. The ROBOTIQ 2F-140 adaptive gripper mounted on the robot's end-effector

TABLE I: Simulation Variables.

Object		Friction	
Type	Box	Model	Stribeck
Dimensions (m)	$[0.1, 0.1, 0.1]$	μ_s	0.6
Weight (kg)	1.0	μ_u (m/sec)	$1.6 * 10^{-5}$
		μ_c	0.52
		k_v $(N * sec/m)$	2.101

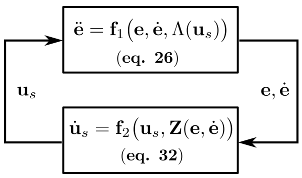

Fig. 3: Feedback Interconnected System.

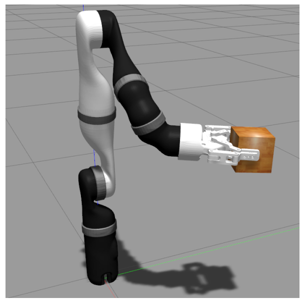

Fig. 4: Simulation Setup.

is grasping a known object with sufficiently large gripping force in order to stabilize it against the gravity in steady state. Then, a desired trajectory is fed to the proposed controller in order to manipulate the object. The friction effect is modeled by the Stribeck friction model which has a continuously differentiable property and can well predict friction both in stick and slip motion [28]. The object properties as well as the friction coefficients are presented in Table I. The values of the friction coefficients are close to the real ones according to the tables in [29].

Due to space limitations, we analyze the case of only one desired trajectory for the interconnected system on 2D plane where slippage occurs on x, y-axis and around z-axis, as depicted in Fig. 11,. Moreover, we compare the results of the proposed control scheme with a classical impedance controller with the same stiffness $\boldsymbol{K}_D = \mathrm{diag}\{5.0, 5.0, 4.5\}$, damping $\boldsymbol{D}_D = \mathrm{diag}\{2.5, 2.5, 2.2\}$ and inertia matrices $\boldsymbol{M}_D = \mathrm{diag}\{0.4, 0.4, 0.3\}$. The variable stiffness and damping gains are $\gamma_k, \gamma_d = 100$, respectively. Moreover, $\alpha = 100$ and $k_s = 10^3$ are the gains of the slippage compensation term $\Lambda(\boldsymbol{v}_s)$.

As it can be observed, the proposed controller has significantly better behavior with respect to slippage effect and simultaneously drives the system to the desired trajectory. In a more detail, the slippage displacement is almost zero along x, y-axis and about z-axis as depicted in Fig. 5, Fig. 6 and Fig. 7. This guarantees that the object and the robot's end-effector follow the same trajectory equal to the desired one Fig. 11.

Moreover, contrary to the classical impedance controller, the proposed control scheme drives the slippage velocity to zero when a small value is measured which guarantees that the object and the robot are moving with the same velocity as Fig. 8 Fig. 9 and Fig. 10 shows. More simulation results can be found in the following video: https://youtu.be/Q5trvGUeKCA.

V. Conclusion

In this work, a model-based variable impedance controller for object manipulation tasks considering non-rigid grasp is presented. The dynamic model of the robot-object interconnected system and the slippage velocity is properly formulated. Then, using Lyapunov based analysis, the desired damping and stiffness matrices, as well as, a slippage compensation term are formulated accordingly in order to guarantee zero convergence for the trajectory error and the slippage velocity assuming that no external forces are acting on the interconnected system. The efficiency of the overall control strategy is verified by conducting a variety of simulation scenarios. Finally, future research efforts will be devoted towards conducting experiments with a real manipulator by developing slip detection tactile sensors (based on [14], [23]), as well as, addressing the problem of non-rigid grasp in cooperative manipulation tasks.

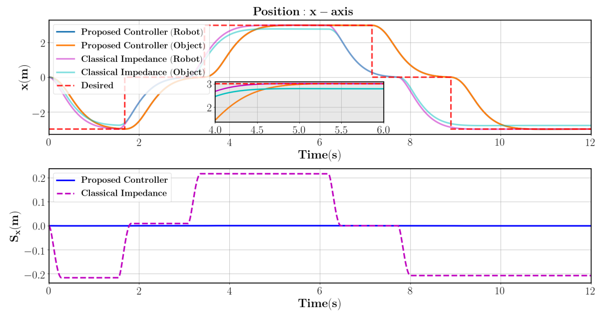

Fig. 5: Position along x-axis.

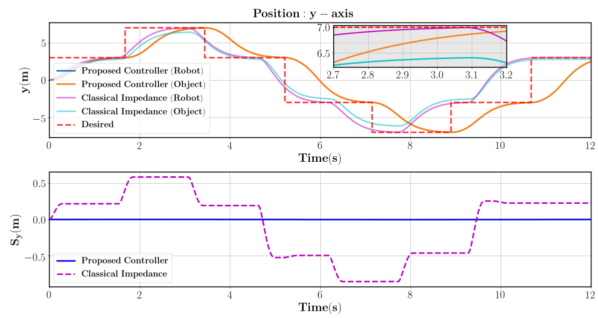

Fig. 6: Position along y-axis.

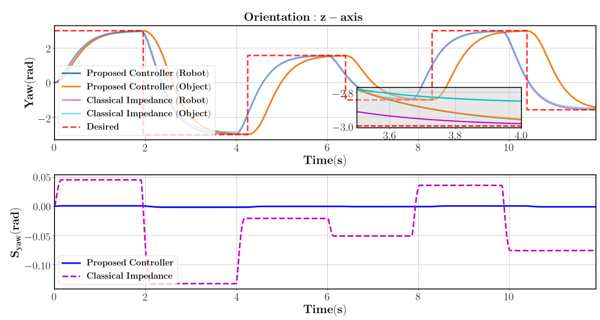

Fig. 7: Orientation about z-axis.

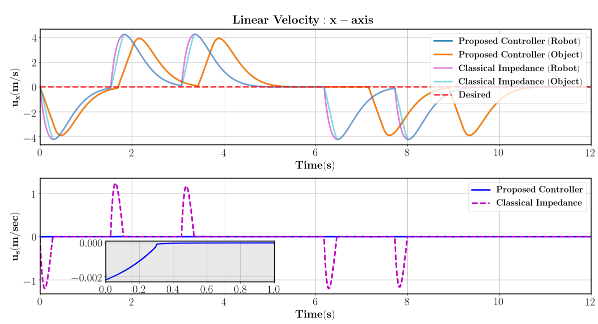

Fig. 8: Linear Velocity on x-axis.

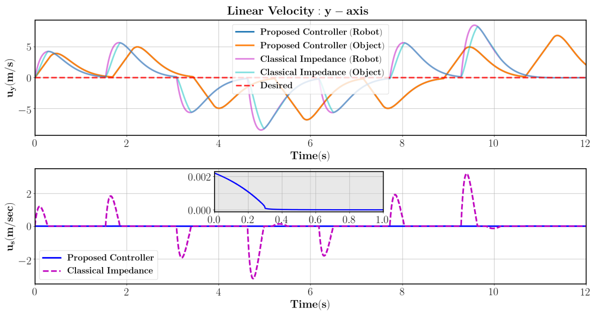

Fig. 9: Linear Velocity on y-axis.

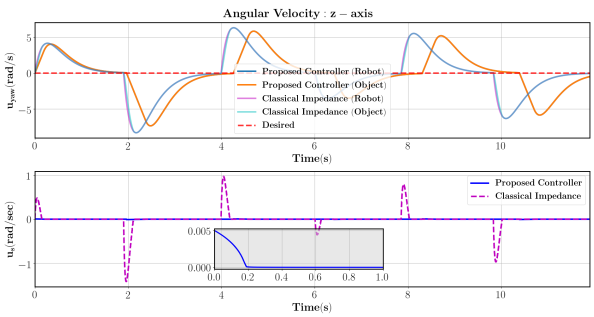

Fig. 10: Angular Velocity about z-axis.

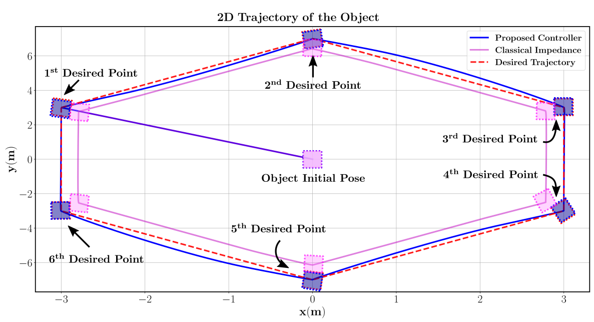

Fig. 11: 2D Trajectory of the Object.

APPENDIX

Lemma 1. *It holds that* $\boldsymbol{x}^\top \boldsymbol{\Phi}_1' \boldsymbol{x} = 0 \, \forall \boldsymbol{x} = [\boldsymbol{x}_1^\top, \boldsymbol{x}_2^\top]^\top \in \mathbb{R}^6$.

Proof.

$$\boldsymbol{x}^\top \boldsymbol{\Phi}_1' \boldsymbol{x} = 2\boldsymbol{x}_1^\top \boldsymbol{S}(\boldsymbol{\omega}_o)\boldsymbol{x}_1 + \boldsymbol{x}_2^\top \boldsymbol{S}(\boldsymbol{\omega}_o)\boldsymbol{x}_2 = 0, \ \forall \boldsymbol{x}_1, \boldsymbol{x}_2 \in \mathbb{R}^3 \Rightarrow \boldsymbol{x} \in \mathbb{R}^6$$

■

REFERENCES

[1] IFR, "Executive summary world robotics 2018 industrial robots," tech. rep., Technical Report, International Federation of Robotics (IFR), 2018.

[2] T. Stock and G. Seliger, "Opportunities of sustainable manufacturing in industry 4.0," *Procedia CIRP*, vol. 40, pp. 536–541, 12 2016.

[3] K.-S. Chang, R. Holmberg, and O. Khatib, "The augmented object model: Cooperative manipulation and parallel mechanism dynamics," in *IEEE International Conference on Robotics and Automation*, vol. 1, pp. 470–475, IEEE, 2000.

[4] H. G. Tanner, S. G. Loizou, and K. J. Kyriakopoulos, "Nonholonomic navigation and control of cooperating mobile manipulators," *IEEE Transactions on robotics and automation*, vol. 19, no. 1, pp. 53–64, 2003.

[5] A. Tsiamis, C. K. Verginis, C. P. Bechlioulis, and K. J. Kyriakopoulos, "Cooperative manipulation exploiting only implicit communication," in *2015 IEEE/RSJ International Conference on Intelligent Robots and Systems (IROS)*, pp. 864–869, IEEE, 2015.

[6] A. Marino, "Distributed adaptive control of networked cooperative mobile manipulators," *IEEE Transactions on Control Systems Technology*, vol. 26, no. 5, pp. 1646–1660, 2017.

[7] A. Marino and F. Pierri, "A two stage approach for distributed cooperative manipulation of an unknown object without explicit communication and unknown number of robots," *Robotics and Autonomous Systems*, vol. 103, pp. 122–133, 2018.

[8] C. K. Verginis, M. Mastellaro, and D. V. Dimarogonas, "Robust cooperative manipulation without force/torque measurements: Control design and experiments," *IEEE Transactions on Control Systems Technology*, 2019.

[9] C. Chi, X. Sun, N. Xue, T. Li, and C. Liu, "Recent progress in technologies for tactile sensors," in *Sensors*, 2018.

[10] R. Lowe, P. Chappell, and S. Ahmad, "Using accelerometers to analyse slip for prosthetic application," *Measurement Science and Technology*, vol. 21, no. 3, p. 035203, 2010.

[11] A. Ikeda, Y. Kurita, J. Ueda, Y. Matsumoto, and T. Ogasawara, "Grip force control for an elastic finger using vision-based incipient slip feedback," in *IEEE/RSJ International Conference on Intelligent Robots and Systems (IROS) (IEEE Cat. No.04CH37566)*, pp. 810–815 vol.1, Sep. 2004.

[12] J. A. Fishel and G. E. Loeb, "Bayesian exploration for intelligent identification of textures," *Frontiers in neurorobotics*, vol. 6, p. 4, 2012.

[13] V. A. Ho, D. V. Dao, S. Sugiyama, and S. Hirai, "Development and analysis of a sliding tactile soft fingertip embedded with a microforce/moment sensor," *IEEE Transactions on Robotics*, vol. 27, pp. 411–424, June 2011.

[14] K. Zhao, X. Li, C. Lu, G. Lu, and Y. Wang, "Video-based slip sensor for multidimensional information detecting in deformable object grasp," *Robotics and Autonomous Systems*, vol. 91, pp. 71–82, 2017.

[15] A. Cirillo, P. Cirillo, G. De Maria, C. Natale, and S. Pirozzi, "Control of linear and rotational slippage based on six-axis force/tactile sensor," in *2017 IEEE International Conference on Robotics and Automation (ICRA)*, pp. 1587–1594, IEEE, 2017.

[16] M. Costanzo, G. De Maria, and C. Natale, "Slipping control algorithms for object manipulation with sensorized parallel grippers," in *2018 IEEE International Conference on Robotics and Automation (ICRA)*, pp. 7455–7461, IEEE, 2018.

[17] N. Chavan-Dafle and A. Rodriguez, "Prehensile pushing: In-hand manipulation with push-primitives," in *2015 IEEE/RSJ International Conference on Intelligent Robots and Systems (IROS)*, pp. 6215–6222, IEEE, 2015.

[18] S. Stepputtis, Y. Yang, and H. B. Amor, "Extrinsic dexterity through active slip control using deep predictive models," in *2018 IEEE International Conference on Robotics and Automation (ICRA)*, pp. 3180–3185, IEEE, 2018.

[19] M. Costanzo, G. De Maria, and C. Natale, "Two-fingered in-hand object handling based on force/tactile feedback," *IEEE Transactions on Robotics*, vol. 36, no. 1, pp. 157–173, 2020.

[20] D. S. Carabis and J. T. Wen, "Slip avoidance in dual-arm manipulation," in *2018 IEEE/RSJ International Conference on Intelligent Robots and Systems (IROS)*, pp. 2872–2879, Oct 2018.

[21] A. Fakhari, M. Keshmiri, and M. Keshmiri, "Dynamic modeling and slippage analysis in object manipulation by soft fingers," in *ASME 2014 International Mechanical Engineering Congress and Exposition*, American Society of Mechanical Engineers Digital Collection, 2014.

[22] S. H. Jazi, M. Keshmiri, F. Sheikholeslam, M. G. Shahreza, and M. Keshmiri, "Adaptive manipulation and slippage control of an object in a multi-robot cooperative system," *Robotica*, vol. 32, no. 5, p. 783802, 2014.

[23] V. A. Ho, T. Nagatani, A. Noda, and S. Hirai, "What can be inferred from a tactile arrayed sensor in autonomous in-hand manipulation?," in *2012 IEEE International Conference on Automation Science and Engineering (CASE)*, pp. 461–468, Aug 2012.

[24] B. Siciliano and L. Villani, *Robot force control*, vol. 540. Springer Science & Business Media, 2012.

[25] F. Caccavale, C. Natale, B. Siciliano, and L. Villani, "Resolved-acceleration control of robot manipulators: A critical review with experiments," *Robotica*, vol. 16, no. 5, pp. 565–573, 1998.

[26] N. Koenig and A. Howard, "Design and use paradigms for gazebo, an open-source multi-robot simulator," in *2004 IEEE/RSJ International Conference on Intelligent Robots and Systems (IROS) (IEEE Cat. No.04CH37566)*, vol. 3, pp. 2149–2154 vol.3, Sep. 2004.

[27] N. McClamroch, "Singular systems of differential equations as dynamic models for constrained robot systems," in *Proceedings. 1986 IEEE International Conference on Robotics and Automation*, vol. 3, pp. 21–28, IEEE, 1986.

[28] Y. Liu, J. Li, Z. Zhang, X. Hu, and W. Zhang, "Experimental comparison of five friction models on the same test-bed of the micro stick-slip motion system," *Mechanical Sciences*, vol. 6, no. 1, pp. 15–28, 2015.

[29] D. D. Fuller, "Coefficients of friction." Avaliable at `https://web.mit.edu/8.13/8.13c/references-fall/aip/aip-handbook-section2d.pdf`.